Tectonophysics 746 (2018) 549–561

Contents lists available at ScienceDirect

Tectonophysics

journal homepage: www.elsevier.com/locate/tecto

The role of lateral strength contrasts in orogenesis: A 2D numerical study

Katharina Vogt[a,*], Ernst Willingshofer[a], Liviu Matenco[a], Dimitrios Sokoutis[a,b], Taras Gerya[c], Sierd Cloetingh[a]

[a] Department of Earth Sciences, Utrecht University, Budapestlaan 6, 3584 CD Utrecht, The Netherlands
[b] Department of Geosciences, University of Oslo, PO Box 1047 Blindern, N-0316 Oslo, Norway
[c] Department of Earth Sciences, ETH-Zurich, Sonneggstrasse 5, 8092 Zurich, Switzerland

ARTICLE INFO

Keywords:
collision zone
numerical modelling
orogenesis
Alps
Pyrenees

ABSTRACT

In this paper we present a series of thermo-mechanical experiments on continent-continent collision zones to investigate the role of lateral strength contrasts in terms of collision dynamics and orogen geometries. Our results show that differences in crustal rheology, may lead to a variety of different patterns of deformation and crustal geometries. Upper plate indentation forms a sequence of foreland propagating thrust units made of brittle upper crust on the lower plate. The strong deformation of the lower plate stands in stark contrast to the undeformed upper plate. In contrast, subduction of strong lithosphere beneath a weak upper plate forms a complex pattern of deformation. Deformation initiates on the lower plate and forms an antiformal stack made of brittle upper crust, before it indents the upper plate. Hence, deformation is present on both, the lower and upper plate, despite differences in initial strength. The outcome of this study has direct implications to natural collision zones, where differences in strength between the upper and lower plate exist. For example, along strike variability of upper vs. lower plate shortening in the Alps are likely to be controlled by contrasts in crustal strength. Furthermore, we suggest that the antiformal stack in the axial zone of the Pyrenees might indicate a strong lower plate at the onset of collision. Our results may therefore provide important constraints for the rheological state of continents during collision.

1. Introduction

Major effort has been made to better understand the dynamics of collisional systems by means of analogue and numerical modelling. It has become increasingly evident that strength contrasts and material heterogeneities have important implications on the deforming mountain belt (i.e.: Beaumont and Quinlan, 1994; Luth et al., 2013a; Willingshofer et al., 2013; Vogt and Gerya, 2014). Both rheological layering of the continental lithosphere (Brun, 2002, Jammes and Huismans, 2012; Jammes et al., 2014; Burov and Yamato, 2008; Burov et al., 2014; Vogt et al., 2017) and weak or strong zones bordering continental domains (Gerbault and Willingshofer, 2004; Willingshofer and Sokoutis, 2009; Sokoutis and Willingshofer, 2011; Gorczyk and Vogt, 2015; Calignano et al., 2015) were shown to affect patterns of stress and the sequence of deformation and, consequently, the overall structure of the orogen, i.e.: geometry, topography and length scale.

However, relatively little attention has been placed upon lateral large-scale contrasts in strength. These may arise when colliding plates have experienced different tectonic or thermal histories or have contrasting material properties. Geological observations suggest that such strength contrasts are present between major continental plates such as India and Asia or Adria and Europe, which resulted in the formation of the Himalayas and the Central and Eastern European Alps, respectively (e.g., Ziegler et al., 1995, 1998; Schoenbohm et al., 2006; Becker and Faccenna, 2011). Even though indentation models representing the collision of strong and weak continental lithosphere have been analysed in numerous analogue and numerical studies, they either focus solely on frictional behaviour (analogue experiments: Bonini et al., 1999; Crespo-Blanc and González-Sánchez, 2005; Luth et al., 2013b), use simplified Newtonian rheologies (analogue multi-layer systems: Davy and Cobbold, 1988; Ratschbacher et al., 1991a; Keep, 2000; Willingshofer et al., 2005) or are restricted to viscous deformation only (numerical viscous thin sheet models: e.g. England and McKenzie, 1982; England and Houseman, 1986; Houseman and England, 1986). Generally, none of these models accounts for the deformation of the indentor or the sub-lithospheric mantle. Only a few studies, using more complex rheologies and setups, have varied the strength of the lower plate to infer its impact on the collisional system (Sokoutis et al., 2005; Luth et al., 2013a; Willingshofer et al., 2013). However, a detailed thermo-mechanically coupled study that analyses strength contrasts

* Corresponding author.
E-mail address: katha_vogt@gmx.com (K. Vogt).

http://dx.doi.org/10.1016/j.tecto.2017.08.010
Received 12 December 2016; Received in revised form 1 August 2017; Accepted 10 August 2017
Available online 12 August 2017

between the upper and lower plate is still missing.

Here we use a 2D numerical high-resolution thermo-mechanical model to investigate the impact of inherited lateral strength contrasts between two colliding plates on the resulting deformation pattern and final geometry. This model comprises a lithospheric to upper mantle cross-section and accounts for complex rheological behaviour that includes viscous creep, plastic yielding and strain softening. Our parametric study is primary focused on influences of two major parameters, which control crustal accretion in collisional zones: (1) the rheological strength contrast between two colliding continental plates and (2) their convergence rate. Additional experiments describing the impact of lithospheric layering on continental collision may be found in Vogt et al. (2017).

2. Methods

Our thermo-mechanical model is based on the I2VIS code of Gerya and Yuen (2003) and is similar to the one discussed in Vogt et al. (2017). The model combines a finite difference approach and a marker in cell technique to solve a series of thermal and mechanical equations. The thermal evolution of the system is modelled by solving the energy equation, which accounts for latent, adiabatic, radiogenic and shear heat production. The equations of mass (continuity equation) and momentum (Stokes equation for slow flow) are solved for a compressible, non-Newtonian, visco-plastic fluid. Elasticity that may alter the short-term stress distribution in our models is not accounted for. However, the numerical formulation provides adequate first-order estimates on the long-term stress evolution of mountain belts that are assembled over millions of years. Details on the basic numerical approach are described in Gerya and Yuen (2003, 2007) and Gerya (2010). The model is designed to study the self-consistent evolution of mountain belts during continent collision on a lithospheric to upper mantle cross-section. This model also accounts for partial melting of different lithologies as described in Vogt et al. (2012).

2.1. Rheology

The viscous creep of rocks (ductile flow) is defined in terms of deformation invariants and depends on temperature, pressure and strain rate. The viscosity for dislocation creep is defined as follows (Gerya, 2010):

$$\eta_{creep} = \frac{\dot{\varepsilon}^{(1-n)/n}}{A_D^{1/n}} e^{\frac{E_a + PV_a}{nRT}}$$

where $\dot{\varepsilon} = \left(\frac{1}{2}\dot{\varepsilon}_{ij}\dot{\varepsilon}_{ij}\right)^{\frac{1}{2}}$ is the second invariant of the strain rate tensor. A_D (pre-exponential factor), E_a (activation energy), n (creep exponent), V_a (activation volume) are experimentally determined flow law parameters and R is the gas constant.

Plasticity is implemented using the following yield criterion, which limits the creep viscosity, altogether yielding an effective visco-plastic rheology (Gerya, 2010):

$$\eta_{creep} \leq \frac{\sigma_{yield}}{2\dot{\varepsilon}_{II}}$$

$$\sigma_{yield} = c + P\sin(\phi)$$

The local plastic strength of a rock depends on the mean stress, P (dynamic pressure), ambient brittle/plastic strength c, which is the strength at $P = 0$, and on ϕ, the effective internal friction angle, which is calculated from the friction angle of dry rocks. The rheologies used in this study are summarized in Table 1.

2.2. Surface processes

The topography of the model (air/crust interface) evolves according to a transport equation. It accounts for sedimentation and erosion and is calculated for each time-step (Gerya, 2010):

$$\frac{\partial z_{es}}{\partial t} = v_z - v_x\frac{\partial z_{es}}{\partial x} - v_s + v_e$$

where z_{es} is the vertical position of the surface as a function of the horizontal distance x; v_z and v_x are the vertical and horizontal components of the material velocity vector at the surface; vs = 0.09 mm/yr and v_e = 0.9 mm/yr are the sedimentation and erosion rates, respectively (e.g. Gerya, 2010).

2.3. Model setup

The computational domain is two-dimensional and covers 1200 km × 600 km (Fig. 1A). The rectangular grid with 1391 × 451 nodal points is non-uniform and contains a (500 km wide and 100 km deep) high-resolution area (0.5 km × 0.5 km) in the centre of the domain. The rest of the model remains at a lower resolution (10 × 4 km). The lower boundary is permeable, satisfying an external free slip boundary condition below the lower boundary of the box (Gerya, 2010). All other boundaries are free slip.

The continental crust has a total thickness of 35 km. It is subdivided into 20 km of upper (felsic) and 15 km of lower (mafic) crust. The upper crust has a quartzite (strong) or wet quartzite (weak) rheology and the lower crust has a plagioclase (weak) or diabase (strong) rheology (Ranalli, 1995), which results in decoupling of upper and lower crust (Vogt et al., 2017). The underlying mantle is composed of dry olivine. A constant velocity rate within a small internal domain of the lithosphere induces horizontal compression between two continental blocks of varying strength (e.g. Gorczyk and Vogt, 2015). We assume that these blocks have undergone different tectonic histories prior to collision, which has resulted in contrasting strength distributions (Fig. 1B). Building on previous numerical models on continent collision we have implemented a weak zone of low plastic and viscous strength that represents a fossil suture zone after ocean closure (Fig. 1). This weak suture zone dips at an angle of 45° beneath the upper plate and provides efficient rheological decoupling between the colliding plates, enabling subduction of the incoming mantle lithosphere beneath the collisional orogen (e.g. Burg and Gerya, 2005; Willingshofer et al., 2013; Vogt et al., 2017).

The thermal boundary conditions are 0 °C at the upper boundary and 0 heat flux across the vertical boundaries. We selected an initial simplified geothermal gradient based on previous studies of continental subduction (e.g., Burov and Yamato, 2008, Vogt et al., 2017). A thermal gradient of 25 °C/km is prescribed for the uppermost 10 km of the continental lithosphere, followed by a lower gradient of 10 °C/km until a temperature of 1330 °C at 118 km depth is reached. This results in Moho-temperatures of 500 °C and a lithosphere-asthenosphere transition zone at 118 km depth. For the asthenospheric mantle a thermal gradient of 0.5 °C/km is used. All material properties are summarized in Table 1.

To allow for topographic buildup of the lithosphere a layer of 20 km of low viscosity (10^{18} Pas) and low density (1 kg/m^3) is implemented above the lithosphere. The large viscosity contrast between this layer and the lithosphere minimizes shear stresses (< 10^4 Pa) making it an efficient free surface. At surface levels this material is exposed to sedimentation (0.09 mm/yr) and erosion (0.9 mm/yr).

2.4. Model limitations

Our models are not capable of reproducing all complexities of natural collisional systems, but are aimed to analyse some of their first order characteristics. Strength contrasts are shown to have profound implications on collision dynamics, but other factors such as variations in temperature, crustal heterogeneities and the presence or absence of fluid and melt may alter the model behaviour. A further shortcoming of this model is, its constant velocity boundary condition. In nature,

Table 1
Material properties. ρ = initial density. Wet qtz = wet quarzite, qtz = quarzite, plag = plagioclase (anorthite 75%), dry ol = dry olivine, wet ol = wet olivine after (Ranalli, 1995, and references therein). AD is the pre-exponential factor, n, is the stress exponent, Ea is the activation energy, Va is the activation volume, φ is the friction angle, and c is the cohesion. Strain weakening is applied within a strain interval of 0–1, at which the friction angle (sin(φ)) and cohesion (c) are decreased. Hr = radioactive heat production, Cp = isobaric heat capacity, α = coefficient of thermal expansion, β = coefficient of thermal compressibility, k = thermal conductivity. A = T[K] + 77; B = 0.00004 × P[MPa].

Properties	Sediment	Upper crust		Lower crust		Mantle	
		Weak	Strong	Weak	Strong	Dry	Shear zone
Flow law	Wet qtz	Wet qtz	Qtz	Plag	Diabase	Dry ol	Wet ol
$1/A_D$ [$Pa^n s$]	1.97×10^{17}	1.97×10^{17}	3.75×10^{19}	4.80×10^{22}	1.26×10^{24}	3.98×10^{16}	5.01×10^{20}
n	2.3	2.3	2.4	3.2	3.4	3.5	4.0
Ea [J]	154×10^3	154×10^3	156×10^3	238×10^3	260×10^3	532×10^3	470×10^3
Va [J/bar]	0.8	0.8	0.8	0.8	0.8	0.8	0.8
sin(φ)	0.20–0.10	0.30–0.15	0.40–0.20	0.30–0.15	0.40–0.20	0.60–0.30	0.10–0.05
C [Pa]	$1 \times 10^{7-6}$	$1 \times 10^{7-6}$	$1 \times 10^{7-6}$	$1 \times 10^{7-6}$	$1 \times 10^{7-6}$	$1 \times 10^{7-6}$	$1 \times 10^{7-6}$
ρ [kg/m^3]	2600	2700	2700	2900	2900	3300	3200
Hr [μW/m3]	2.0	1.8		0.18		0.022	
Cp [J/kgK]	1000	1000		1000		1000	
α [1/K]	3×10^{-5}	3×10^{-5}		3×10^{-5}		3×10^{-5}	
β [1/MPa]	1×10^{-5}	1×10^{-5}		1×10^{-5}		1×10^{-5}	
k [W/m/K]	[0.64 + 807/A] × exp.(B)	[0.64 + 807/A] × exp.(B)		[1.18 + 474/A] × exp.(B)		[0.73 + 1293/A] × exp.(1 + B)	

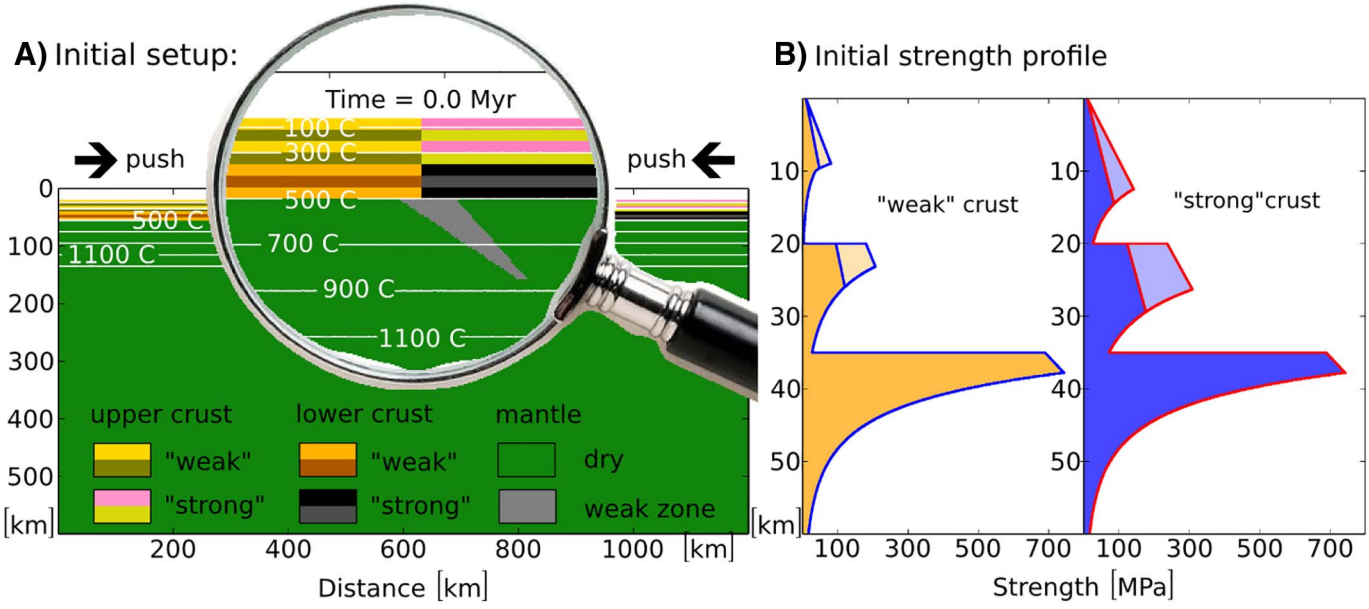

Fig. 1. A) Cross-section of the initial setup. B) Initial strength profiles of the continental lithosphere used in numerical experiments (the profiles are computed for a constant strain rate of $\dot{\varepsilon} = 10^{-14}$ 1/s, which is strongly variable in models, Figs. 2–7). In A and B, the upper plate is shown to be strong, but the exact configuration of weak and strong depends on the experiment. Strain weakening is applied within a strain interval of 0–1, which results in lower plastic strength as shown by the blue and orange shaded area. See Table 1 for all material properties. (For interpretation of the references to colour in this figure legend, the reader is referred to the web version of this article.)

convergence velocities may vary in time ranging from positive to negative.

3. Results

We investigate the physical processes in continent collision zones and its implications to crustal scale deformation and geometry. First, we will consider collision of two equally strong continental plates, separated by a weak suture zone at the base of the crust as described in Vogt et al. (2017) (Fig. 3). Second, we will demonstrate how lateral strength contrasts may alter the evolving deformation pattern, resulting in a variety of different geometries. A summary of all experiments is given in Table 2.

3.1. Experiment A: continental subduction

Experiment A explores the collision of two equally strong continental blocks during slow (A1) and fast (A2) convergence. It defines our reference model to which later experiments will be compared. The results of this experiment have also been described in Vogt et al. (2017) (Fig.3).

Table 2
List of numerical experiments.

Experiment	Lower plate	Upper plate	Convergence rate [cm/yr]
A1	Weak	Weak	0.5
A2	Weak	Weak	5.0
B1	Weak	Strong	0.5
B2	Weak	Strong	5.0
C1	Strong	Weak	0.5
C2	Strong	Weak	5.0

3.1.1. Experiment A1: slow convergence: 0.5 cm/yr

At the onset of collision, two oppositely dipping shear zones (1. pop-up) develop, followed by a lithospheric-scale thrust and a second pop-

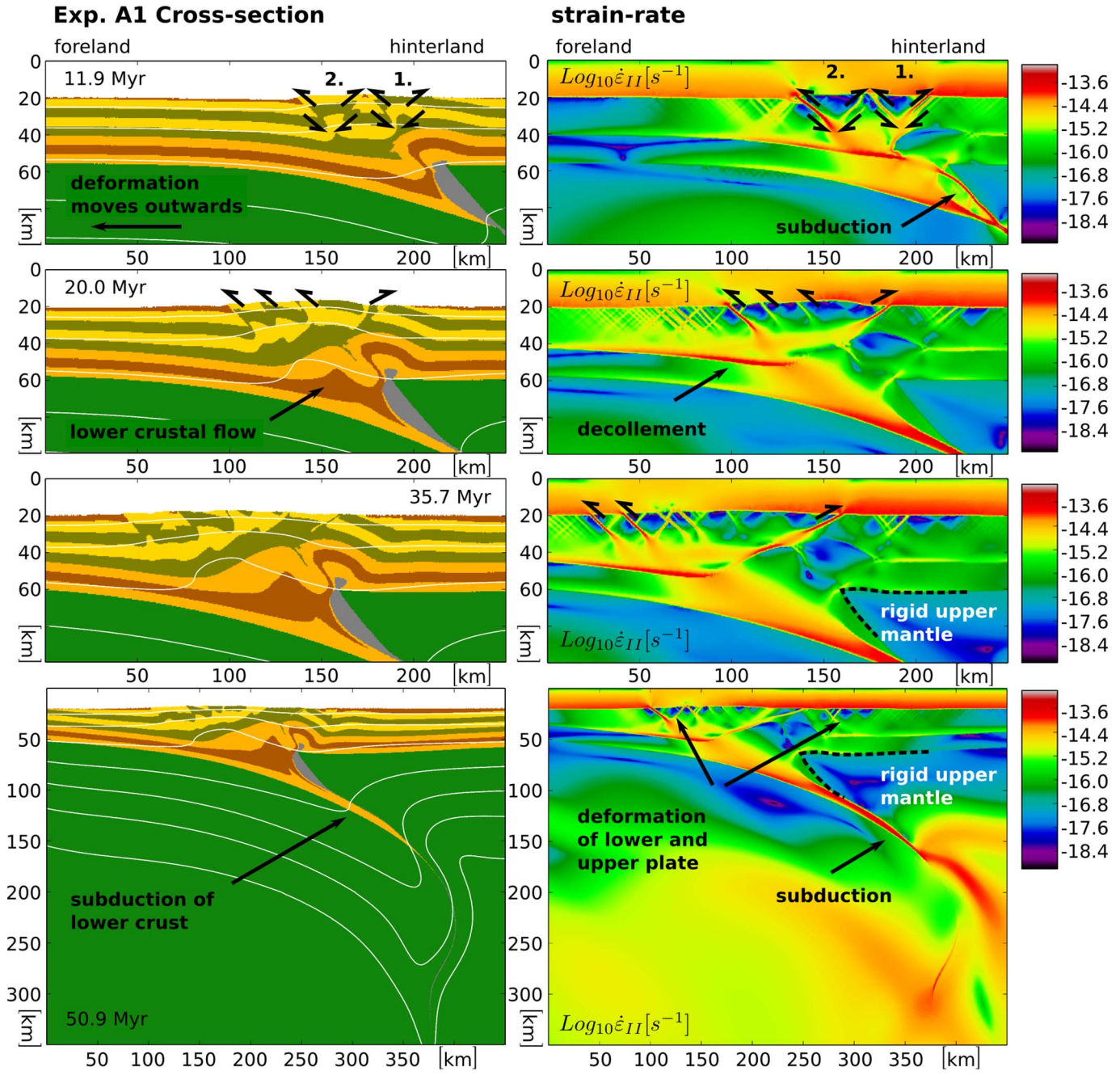

Fig. 2. The left panel shows a cross-section of experiment A1. The corresponding deformation pattern (second strain invariant) is shown in the right panel. Cool clours indicate low values of deformation; warm colours indicate strong deformation. The same colour scheme applies to all figures. Deformation initiates above the weak suture zone, but moves towards the incoming plate shortly after. The upper crust of the lower plate decouples and forms a foreland propagating thrust system. The lower crust of the lower plate subducts and accretes against a backstop made of brittle upper mantle (dashed line). Finally, a back-thrust develops opposite to the main thrust system. The thick black arrows indicate thrusting of the upper crust. Same symbols apply to all figures.

up at 11.9 Myr (Fig. 2). Subsequently, the deformation front migrates towards the lower plate (incoming plate) and activates a sequence of foreland propagating imbricate thrust sheets after 20 Myr (Fig. 2). Because of the weak rheological coupling of upper and lower continental crust, a décollement develops along which basal detachment is feasible. The upper crust decouples from the lower crust and mantle and adopts its own style of deformation, forming a sequence of outward propagating thrusts. Elevated temperatures at the core of the orogen enable lower crustal flow towards the upper plate, evident by the broad zone of distributed deformation in Fig. 2 (domain with similar strain at 20 Myr). Subsequently, the lower crust accretes against a backstop made of brittle upper mantle, which forces the upper plate upwards. This activates a back-thrust above the former suture zone, opposite to the main foreland propagating thrust system (Fig. 2). Hence, the orogen grows and thickens through the imbrication of thrust sheets at the front of the orogen in near surface regions and lower crustal flow at its base. This results in sequential deformation in the foreland and continuous movement along the major back-thrust. In contrast, deformation on the upper plate is more diffuse and less profound. The upper plate is passively uplifted and shows only minor deformation (i.e. minor back-thrusting and pop-up structures after 35.7 Myr, Fig. 2).

At greater depth, parts of the lower crust that have remained coupled to the mantle subduct together with the mantle lithosphere. However, subsequent thermal weakening of the slab (at subcrustal

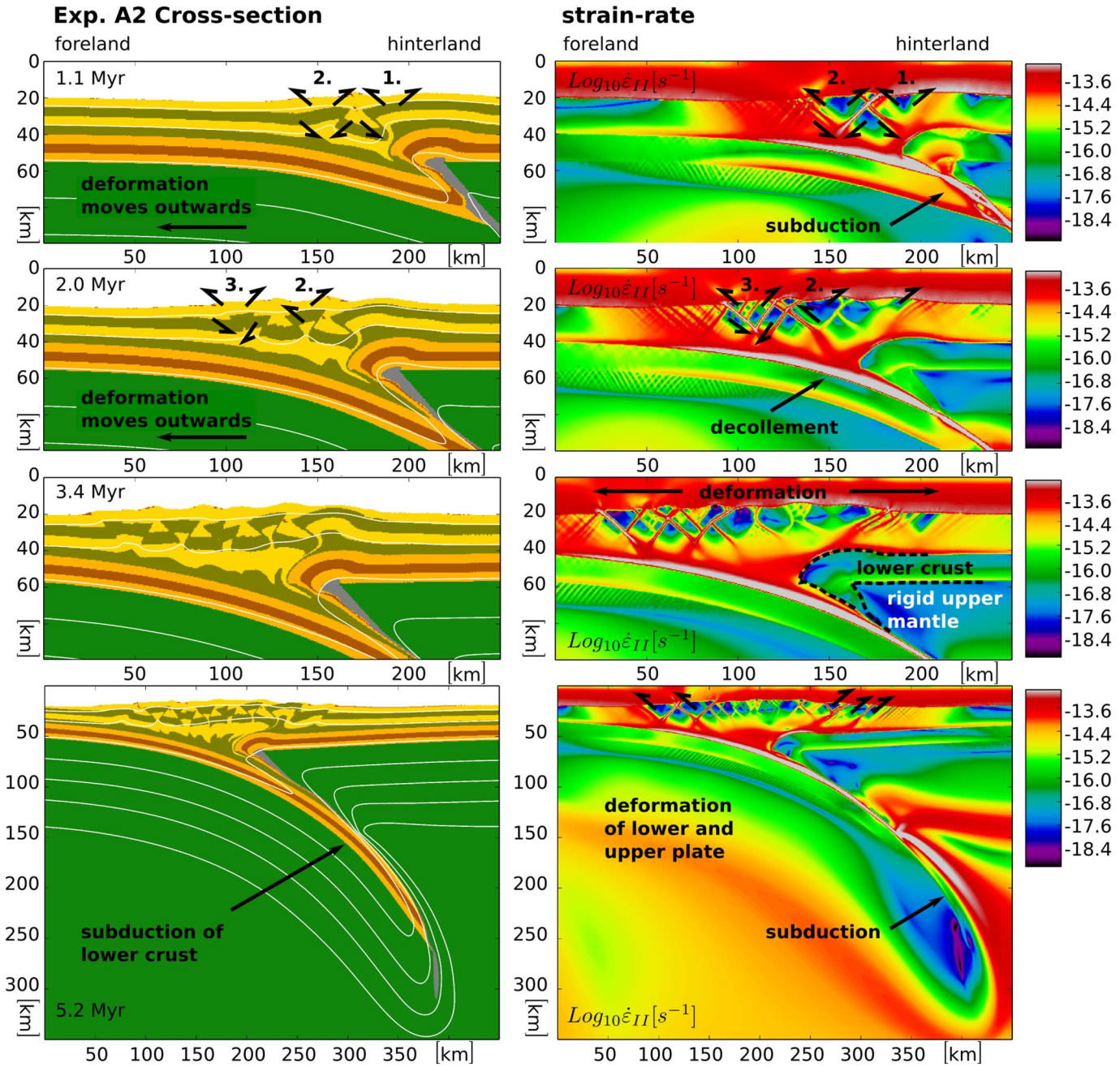

Fig. 3. The left panel shows a cross-section of experiment A2. The corresponding deformation pattern (second strain invariant) is shown in the right panel. Deformation initiates above the weak suture zone, but moves outwards shortly after. The upper crust of the lower plate decouples from the slab and forms a foreland propagating thrust system, unlike the lower crust, which remains coupled to the mantle and subducts. The upper crust of the upper plate forms a thrust system with opposite vergence. In contrast, the lower crust of the upper plate remains nominally undeformed. The black dashed line shows the outline of the upper plate (crust and brittle upper mantle).

depth) prevents further subduction and promotes lower crust accretion. This leads to low coupling of the upper and lower plate and forms a shallow dipping slab and a wedge shaped Moho (Fig. 2).

3.1.2. *Experiment A2: fast convergence: 5.0 cm/yr*

The early stages of collision are similar to A1. Deformation localizes within the suture zone and propagates towards the lower plate after 1–2 Myr (Fig. 3). On-going convergence activates a décollement on the lower plate close to the boundary between upper and lower crust. The upper crust decouples and forms a sequence of outward propagating pop-up structures. In contrast to A1, the lower crust remains coupled to the mantle and subducts beneath the rigid lower crust and brittle upper mantle (of the upper plate), because of the cool inner core of the orogen. No major back-thrust is formed; instead shortening is accommodated on both plates by outward (into the undeformed fore- and hinterland; Fig. 3) propagating thrusts above an upper crustal décollement between 3.4 and 5.2 Myr. In this model the crust thickens because of the constant accretion of upper crust material, either by imbricate thrusts in the brittle domain or by flow and folding in the ductile domain (Fig. 3 after 5.2 Myr). Because of the fast subduction velocity, the slab has no time to heat up and weaken. It preserves its strength and steepens as it sinks into the mantle.

3.2. *Experiment B: strong upper plate*

In experiment B1 (slow convergence) and B2 (high convergence) we

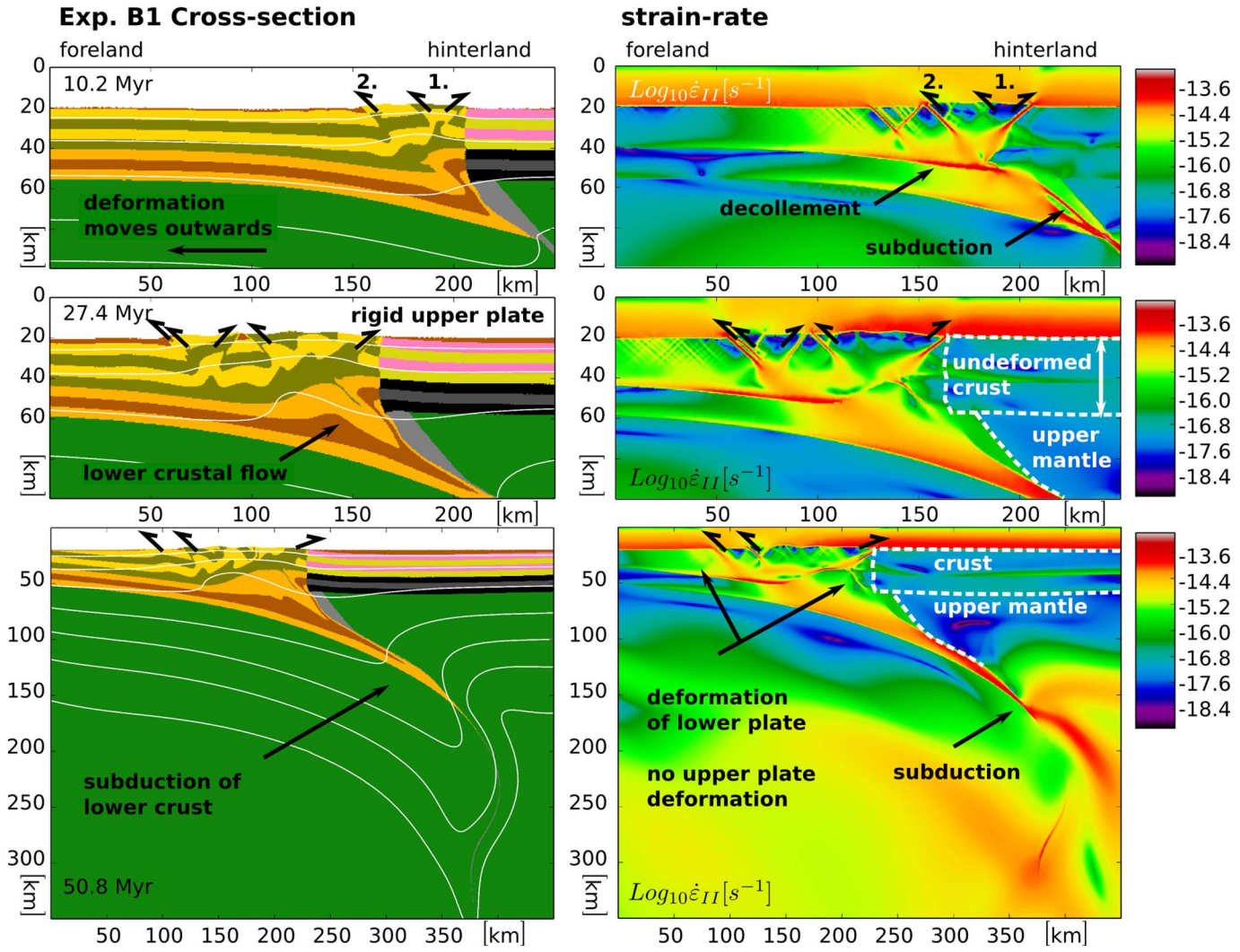

Fig. 4. The left panel shows a cross-section of experiment B1. The corresponding deformation pattern (second strain invariant) is shown in the right panel. The degree of deformation varies significantly along the plate interface. The lower plate is subjected to intense deformation in contrast to the upper plate, which remains mostly undeformed throughout the entire model evolution. The white dashed line shows the outline the upper plate (crust and brittle upper mantle). The model evolution is similar to A1.

analyse the collision between two different continental blocks – a weak lower plate and a strong upper plate. The model design is similar to A. The only difference is the high crustal strength (viscous and brittle) of the upper plate.

3.2.1. Experiment B1: slow convergence 0.5 cm/yr

Similar to A1, deformation in B1 is asymmetric – diffuse in the foreland and localized towards the hinterland (Fig. 4 at 10.2, 27.4 and 50.8 Myr). The foreland is characterized by a sequence of foreland vergent thrust sheets (foreland breaking thrust system). In contrast, at the plate contact deformation is accommodated by a major and highly localized, hinterland-vergent back-thrust after 27.4 Myr. Similar to A1 accretion of the lower plate occurs above and below a décollement at the boundary of upper and lower crust. This décollement connects with the major back-thrust as deformation progresses (Fig. 4, after 50.8 Myr). It separates the accretion of brittle upper and ductile lower crust against the rigid upper plate, which remains essentially undeformed (Fig. 4). However, the resulting slab and crustal geometry are comparable to A1 (Fig. 4 at 50.8 Myr).

3.2.2. Experiment B2: fast convergence: 5.0 cm/yr

In experiment B2 fast collision forms a sequence of foreland propagating pop-up structures made of brittle upper crust (Fig. 5 at 1.1, 2.4 and 5.2 Myr). In this experiment, a back-thrust develops in front of the indenter at 2.4 Myr. It maintains its dip attitude and connects at depth with the major decoupling horizon of the incoming plate. The slab preserves its strength and transports the attached lower and to minor extends upper crust down to sublithospheric depth at 5.2 Myr. No lower crust accretion is observed and the growth of the orogen is solely attributed to the upper crust of the lower plate. This stands in strong contrast to the rigid upper plate that remains mostly undeformed throughout the entire model evolution. The final crustal geometry and slab geometry is highly asymmetric after 5.2 Myr of collision, in contrast to A2 (Fig. 5).

3.3. Experiment C: strong lower plate

Experiments C1 and C2 investigate a contrasting end-member to B1 and B2. In these experiments the lower plate has a higher brittle and viscous strength with respect to the upper plate. This difference in strength has profound implications on the collision dynamics and the crustal geometry.

3.3.1. Experiment C1: slow convergence rate 0.5 cm/yr

Similar to all previous experiments, deformation localizes along the weak suture zone and moves towards the foreland (Fig. 6 at 8.2 and

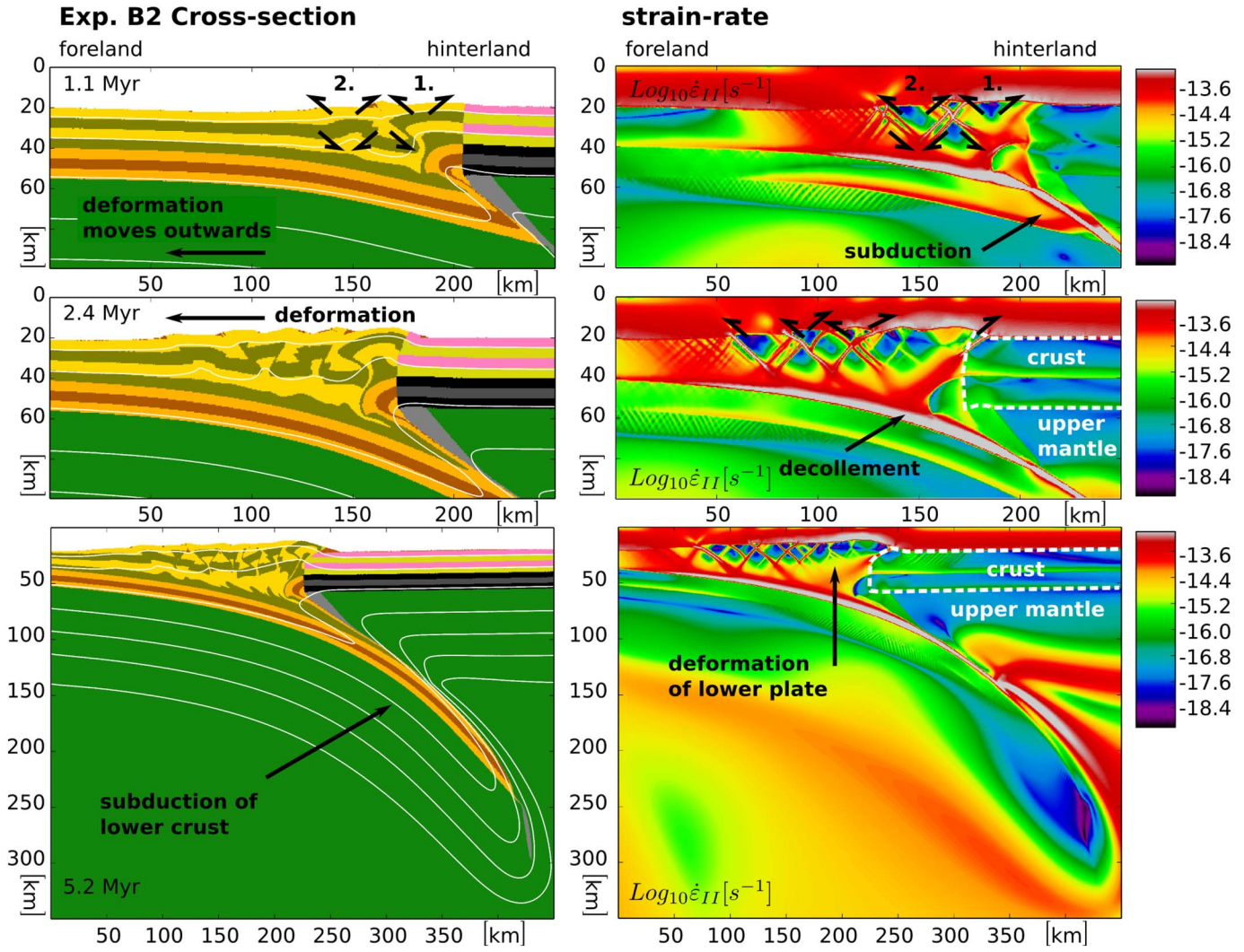

Fig. 5. The left panel shows a cross-section of experiment B2. The corresponding deformation pattern (second strain invariant) is shown in the right panel. Similar to B1, the lower plate shows a significantly higher degree of deformation compared to the upper plate. The white dashed line shows the outline of the upper plate (crust and brittle upper mantle).

18.9 Myr). The upper crust of the lower plate detaches from the downgoing lower crust and lithospheric mantle and forms an antiformal stack (sequence of overlapping thrusts), which accommodates most of the shortening. Deformation is stationary and does not propagate further into the foreland. The successive nucleation and accretion of individual thrusts forces the thrust system upwards and activates a major back-thrust at the boundary between the upper and lower plate. During the first 20 Myr of shortening the upper plate, yet initially weaker, acts as a buttress against which the stack of lower plate thrusts is accreted (Fig. 6). Accretion of the lower plate comprises brittle deformation of the upper most crust and ductile flow at mid-crustal levels. In the course of this process, the thrust system rotates and is subsequently shunted across the plate boundary. Deformation propagates into the undeformed upper plate and forms a sequence of thrusts above a mid-crustal décollement (Fig. 6). In contrast, the lower crust of the upper plate remains mostly undeformed and indents the thermally weakened orogenic wedge at its base between 30 and 50 Myr (Fig. 6). This leads to a situation, where the upper crust of the lower plate is overlying the lower crust of the upper plate. At sub-crustal levels, the strong coupling of lower and to minor extends upper crust and mantle promotes subduction of continental crust. The final configuration differs significantly from all previous examples. The resulting orogen is narrow and displays a complex pattern of deformation that involves rocks of the upper and lower plate.

3.3.2. *Experiment C2: fast convergence rate: 5.0 cm/yr*

The early stages of collision are comparable to those described in C1. Collision initiates deformation within the lower plate and forms a thrust system resembling an antiformal stack made of brittle upper crust during the first 5 Myr (Fig. 7). Different to C1, deformation is truly brittle and the spacing of individual thrusts is greater. The continued accretion of thrust sheets between 3 and 5 Myr forces the thrust system upwards. The individual thrusts rotate gradually and indent the upper plate, deforming the upper and lower crust. The cold crustal wedge inhibits lower crust indentation, as observed in experiment C1 and deformation moves into the undeformed hinterland (Fig. 7 at 5.5 Myr). Consequently, a new thrust system with opposite vergence forms on the upper plate. At subcrustal levels, the strong coupling between crust and mantle, results in continental subduction, but in contrast to all previous examples subduction also comprises significant amounts of upper crust. Slivers of upper crust are dragged to mantle depth, heat up and melt (Fig. 7 at 5.5 Myr). An assemblage of granitic rocks composed of partially molten and solid components forms where temperatures exceed 700 °C at depth of around 100–150 km. Its low density and viscosity enables rapid (2.5–5 cm/yr) return flow along the subduction zone interface. Subsequent movement within the crust (2 cm/yr) leads to crustal reworking and forms a 10 km wide zone of highly sheared rocks between 7 and 8.4 Myr (Fig. 7). The final pluton has a granitic composition and a circular shape of 30 km in size.

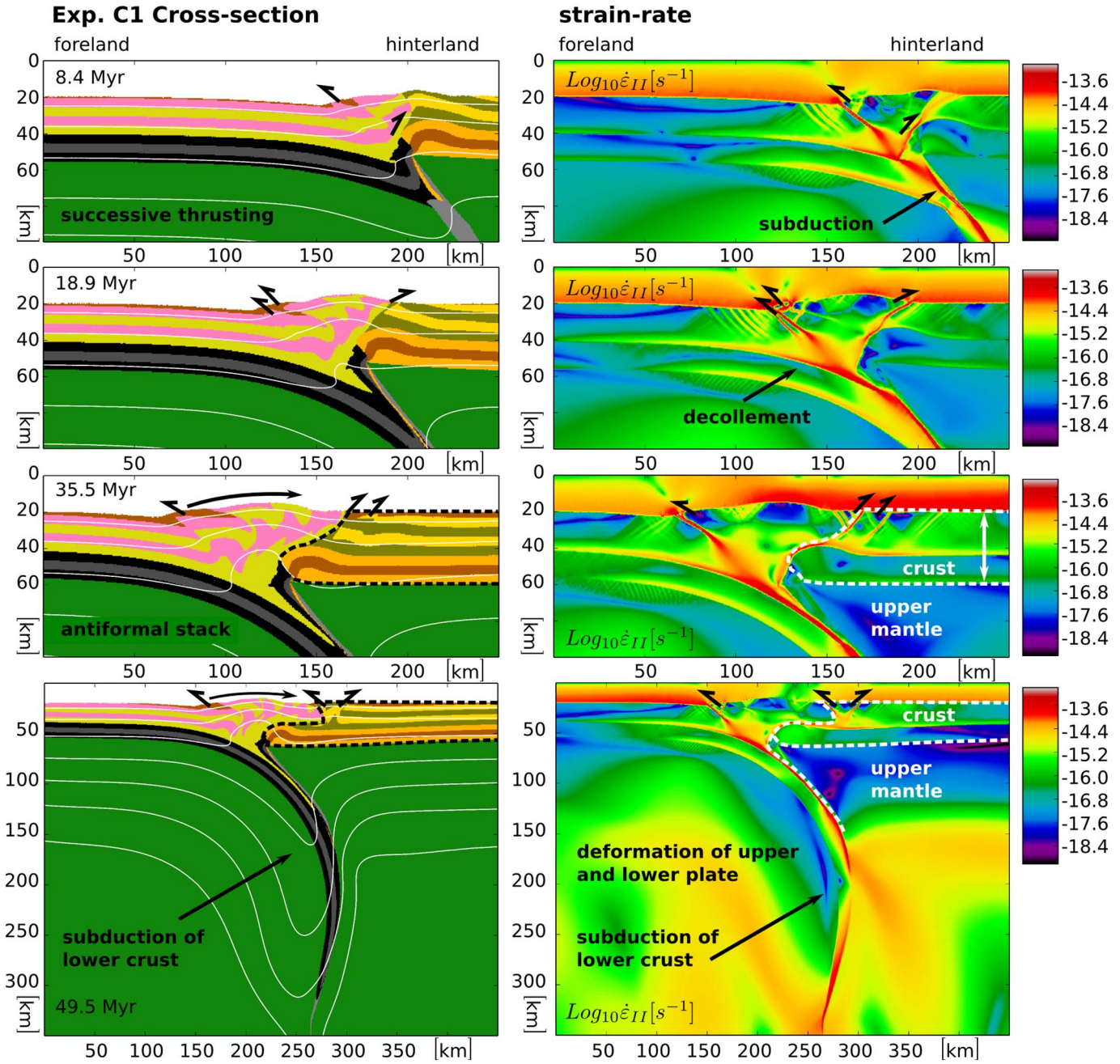

Fig. 6. The left panel shows a cross-section of experiment C1. Deformation forms an antiformal stack made of upper crust of the lower plate. The stack indents the upper crust of the upper plate. The resulting geometry is complex. The upper crust of the lower plate is overlying the lower crust of the upper plate. The dashed line outlines the crust of the upper plate.

4. Discussion

4.1. Collision geometries

4.1.1. Vertical contrasts in lithospheric rheology

Despite many differences in the evolution and final geometry of our experiments, all show lithospheric-scale thrusting followed by subduction of continental lithosphere. This is related to the high strength contrast between the brittle upper mantle (where highest strength resides) and the weak suture zone. Both numerical and analogue studies have demonstrated that continental subduction is critically controlled by the degree of plate (de)coupling (Brun, 2002; Willingshofer and Sokoutis, 2009; Sokoutis and Willingshofer, 2011; Faccenda et al., 2008; Luth et al., 2010, 2013a, Willingshofer et al., 2013). Strong decoupling at the plate contact facilitates continental subduction as shortening is mostly accommodated along the weak plate interface resulting in minor deformation of the upper plate (Faccenda et al., 2008; Luth et al., 2010, 2013a; Willingshofer et al., 2013). However, long-lasting continental subduction requires, moreover, cold initial geotherms (Moho < 550C), rapidly sinking plates (> 3–5 cm/yr) and strong coupling of crust and mantle (Toussaint et al., 2004, Burov and Yamato, 2008; Burov et al., 2014, Vogt et al., 2017). In contrast, thermal diffusion during slow convergence or low rheological coupling of crust and mantle inhibits continental subduction (Toussaint et al., 2004; Burov and Yamato, 2008; Burov et al., 2014; Vogt et al., 2017). Also in nature, subduction of continental lithosphere may comprise the lower continental crust (e.g. Roure et al., 1989; Schmid et al., 1996; Schmid and Kissling, 2000; Pfiffner, 2014; Schneider et al., 2013); a behaviour shown to be strongly controlled by the rheological stratification of the continental crust (e.g. Toussaint et al., 2004; Burg and

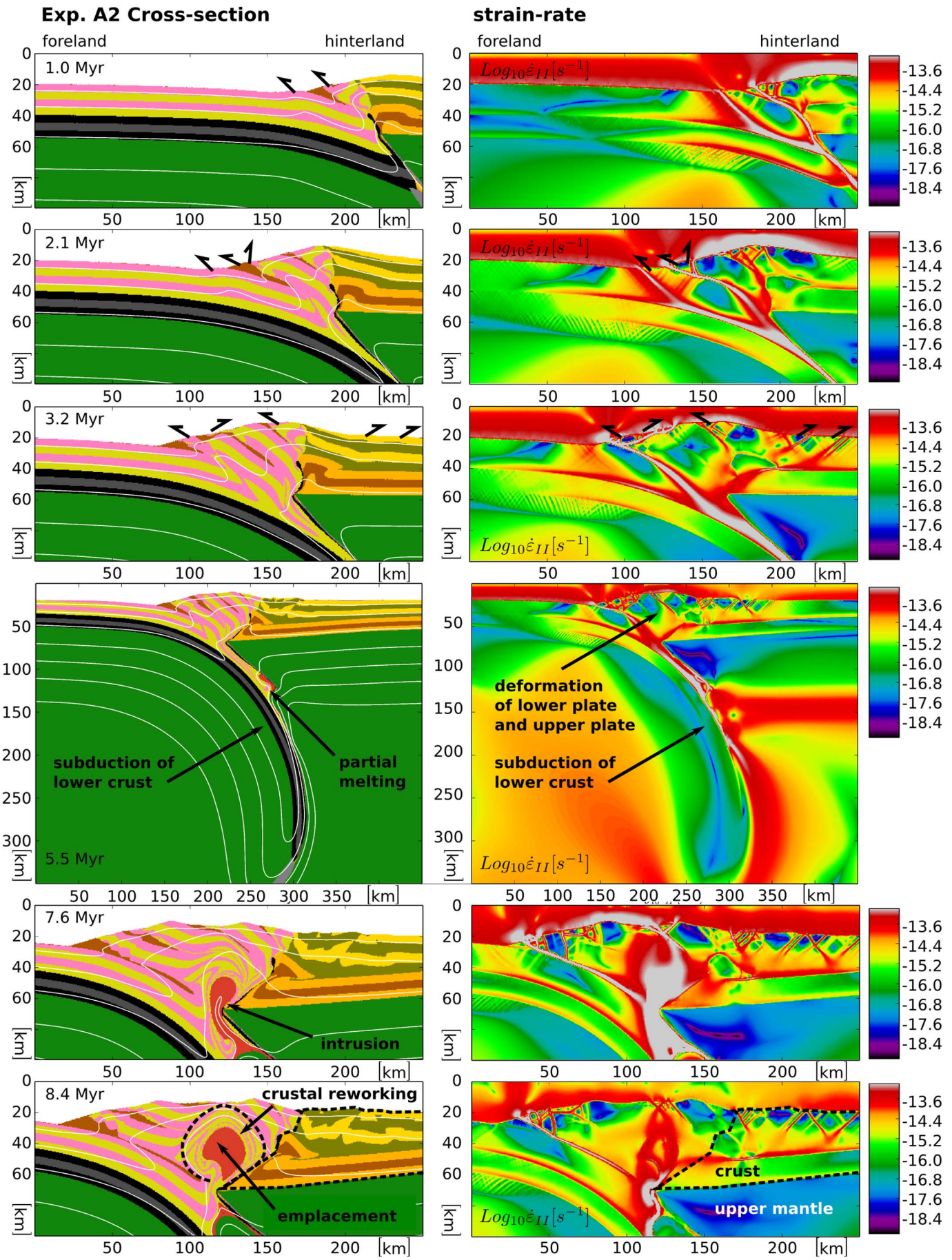

(caption on next page)

Fig. 7. The left panel shows a cross-section of experiment C2. Similar to C1 deformation of the upper crust of the lower plate forms an antiformal stack, which moves onto the upper plate. The upper plate deforms forming a thrust system with opposite vergence. The dashed line outlines the crust of the upper plate. Parts of the upper crust of the lower plate that have bypassed the collision zone melt at depth. This melt rises along the former subduction zones and intrudes the crust.

Gerya, 2005; Burov and Yamato, 2008; Burov et al., 2014; Vogt et al., 2017).

Another commonality is the decoupling of upper and lower crust that is present in all of our experiments. The upper crust adopts its own style of deformation (i.e. outward propagating thrusts or pop-ups in the brittle- and flow in the ductile domain) and shows no simple relation with the mantle lithosphere, which is in agreement with previous modelling studies comprising weak decoupling horizons (e.g. Brun, 2002; Luth et al., 2010, 2013a; Jammes and Huismans, 2012; Jammes et al., 2014; Vogt et al., 2017). In nature, decoupling at the base of the upper crust might be related to strength reduction in quartz owing to higher temperatures, the break-down of feldspar and the associated phyllonite formation, or the effect of fluid overpressure (Pfiffner, 2016). As a consequence deformation is dominated by flow processes resulting in a fold-like geometry at the boundary between upper and lower crust (Fig. 8a–d) as suggested for the European Alps (Pfiffner, 2016).

Fig. 8a,e compares experiment A2 with the work of Luth et al. (2013a) on continental subduction. Despite differences in the plate configuration (i.e. depth of the weak layer) the pattern of deformation and the resulting geometry bears many similarities: The uppermost crust forms a sequence of outward propagating thrusts on the upper and lower plate while the continental lithosphere is dragged into the mantle. However, the pattern of deformation is shown to change as convergence varies. For example, in slow convergence experiments A1 and B1 the successive accretion of thrust-sheets at the front of the orogen is accommodated by the steady offset along a back-thrust with opposite vergence (Figs. 2 and 4). Movement along the back-thrust transports lower crust material to shallower depth, forming the core of the orogen. In contrast, fast convergence experiments A2 and B2 are characterized by a sequence of outward propagating pop-up structures on the upper and lower plate (Figs. 3 and 5). Strain is compensated (i.e. accommodated) for each structure and no major back-thrust is formed. The lower crust subducts along with mantle lithosphere and the orogenic wedge is made up of upper crust material only. This contrasting behaviour is controlled by the relative strength and thickness of the crustal layers and the mantle, and thus, the degree of coupling among them (e.g.: Liu et al., 1992; Brun, 2002; Ellis et al., 2004; Ruh et al., 2012; Vogt et al., 2017).

4.1.2. Lateral contrasts in lithospheric rheology

The strength of the lithosphere controls the pattern of deformation and overall geometry of the orogen. While lithospheric thrusting determines the early stages of collision in all of our experiments, subsequent deformation is critically controlled by differences in crustal strength between the upper and lower plate (e.g., Fig. 8 a–d).

Upper plate indentation in B (Figs. 4, 5) forces deformation to migrate towards the foreland, leaving the upper plate undeformed, which is in accordance with previous studies (Pfiffner et al., 2000; Luth et al., 2013a; Willingshofer et al., 2013; Calignano et al., 2015). Fig. 8b,f compares experiment B2 with the work of Willingshofer et al. (2013) on continental collision: Both examples show upper plate indentation and lower plate deformation.

In contrast, subduction of a strong lower plate beneath a weak upper plate in C results in a more complex pattern of deformation (Figs. 6, 7). Deformation initiates on the lower plate forming an antiformal stack. Part of this structure is subsequently transferred to the upper plate such that the upper crust of the lower plate is thrust on top of the lower crust of the upper plate, while the latter is moved beneath the lower plate (Figs. 6, 7). These observations are in agreement with earlier numerical studies that have investigated the effect of a weak midcrustal layer in an overall brittle upper plate during continental collision (Pfiffner et al., 2000). In the work of Pfiffner et al. (2000), detachment of the upper crust activates a crustal-scale syncline on the upper plate. Subsequent deformation migrates further into the undeformed upper plate, but leaves the lower crust nominally undeformed, giving it the geometry of an apparent lower crust indenter (Pfiffner et al., 2000). Despite differences in the model setup and computational strategy, the basic features observed in C1 (Fig. 6) are in agreement with the work by Pfiffner et al. (2000). The difference in thrust spacing and offset between C1 (slow convergence: Fig. 6) and C2 (high convergence: Fig. 7) is related to differences in convergence velocity, and therefore, crustal strength. Previous studies have shown that deformation of weak crust forms thick-skinned crustal scale thrusts, while deformation of strong crust forms long thrust sheets, which is in agreement with our work (Jammes and Huismans, 2012; Vogt et al., 2017).

4.2. Relevance of 2D modelling results for natural 3D collision systems

In this section we discuss the relevance of our modelling results (Fig. 8a–d) with respect to key elements of the European Alps and the Pyrenees as these orogens (Fig. 8g–j) are very well constrained by geophysical and geological data and observations (e.g. Schmid et al., 1996, 2004; Schmid and Kissling, 2000; Kissling et al., 2006; Transalp Working Group, 2002; Diehl et al., 2009 Wagner et al., 2012; Zhao et al., 2015; Pfiffner, 2016; Choukroune, 1989; Roure et al., 1989; Muñoz, 1992; Teixell, 1998; Wang et al., 2016), which revealed that both orogenic systems are highly non-cylindrical. Our discussion is focussed on the rheology controlled deformation geometries of the upper and the lower plate.

4.2.1. Distribution and style of deformation in response to plate rheology

Recent quantitative studies have shown that the along strike variability of upper vs. lower plate shortening in the Central Alps reflects lateral heterogeneities of the plates involved in Alpine collision (e.g. Rosenberg and Kissling, 2013). In particular, Rosenberg and Kissling (2013) have suggested that lateral changes in temperature controlling the rheology and degree of crustal coupling explain the shift of upper plate (west) to lower plate (east) indentation in the Alps. Furthermore, in the eastern Alps indentation of the orogenic wedge probably occurred on the scale of the upper crust, which decoupled form the subducting mantle lithosphere (Lippitsch et al., 2003) during the Early Miocene. As such, rheological changes across strike of the orogen reside within the crust and are a consequence of different tectonothermal ages of the Eastern Alps (Austroalpine) crust as opposed to the Adriatic crust (Willingshofer and Cloetingh, 2003). Our experiments show that in cases where the upper plate is significantly stronger at the onset of collision (Figs. 4, 5), almost all deformation resides in the weak lower plate and only minor backthrusting is observed close to the contact of the plates. In the Alps such partitioning of deformation is observed in the western Alps (compare Fig. 8d and i–j), where the Ivrea body acts since the Late Oligocene as a strong buttress against which lower plate material is accreted (Handy et al., 1999; Schmid et al., 1996; Pfiffner, 2014; Schmid et al., 2017). Under such conditions, a clear correlation between plate strength and the localization of deformation (dominantly in the lower plate) exists. When the lower plate is strong, more deformation is observed in the upper plate and in particular its upper crust, which is bulldozed by the stacked lower plate units (Figs. 6, 7). Nevertheless, most of the shortening occurs in the lower plate similar to experiments comprising a strong upper plate (Figs. 4 and 5). Thus, no direct correlation exists between plate strength and the partitioning of upper plate-lower plate deformation in cases, where the locus of deformation is strongly controlled by the kinematics

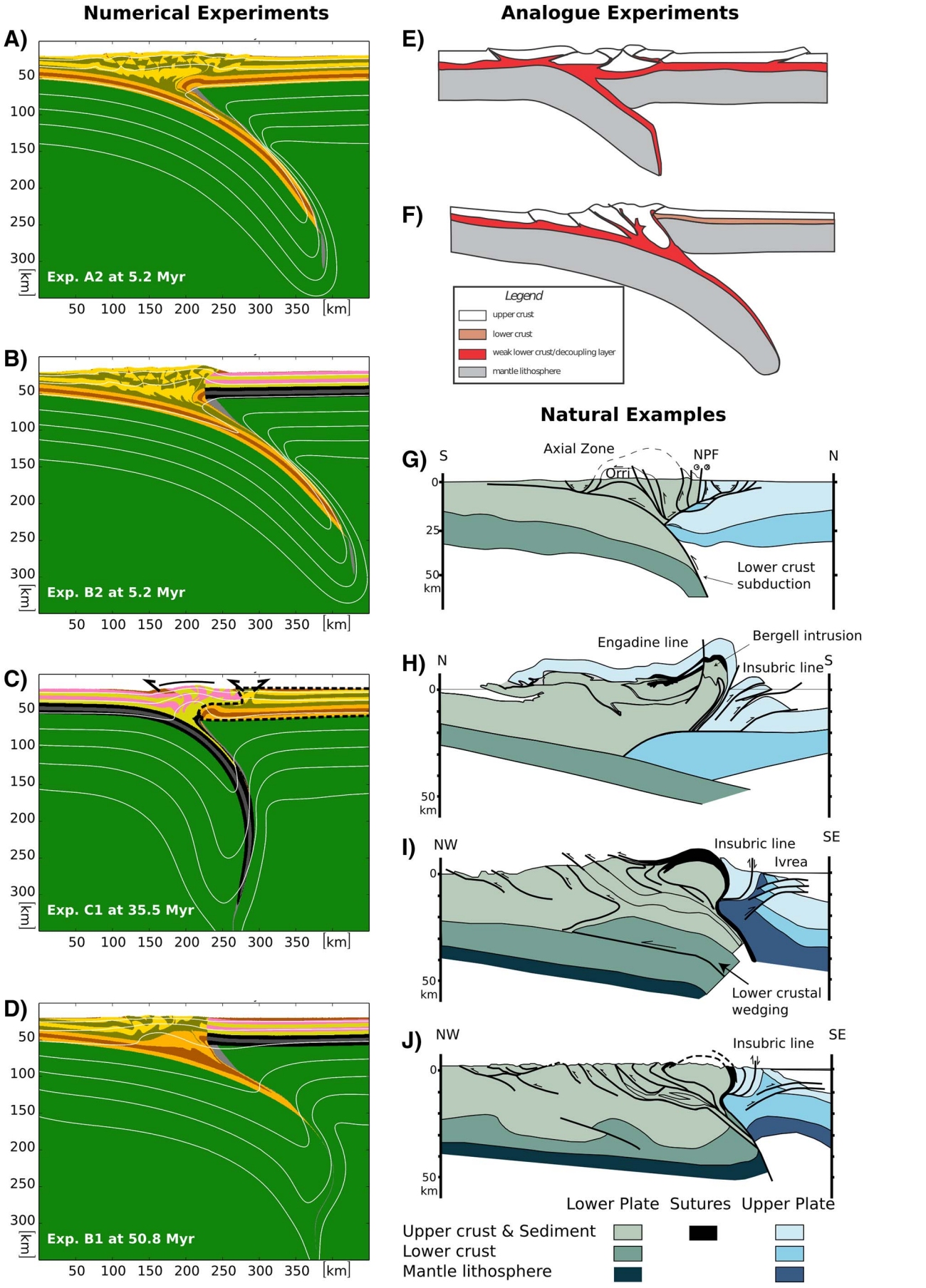

(caption on next page)

Fig. 8. Comparison of model results a–d) with selected analogue e–f) and natural examples g–j). a–d) We refer to the text for a detailed description of Exp. A2, B2, C1 and B1. e) and f) Analogue experiment on continental collision with two equally strong plates (e) and a stronger upper plate (f), modified from Luth et al., 2013a and Willingshofer et al., 2013, respectively. Note their close resemblance with our experiments A2 and B2. g) Crustal cross-section across the Pyrenean chain (modified after Muñoz, 1992). The overall geometry (i.e., antiformal stack in the axial zone) is similar to experiment C1. h), i) and j) Crustal cross section across the Central and Western Alps, respectively (modified after Schmid et al., 2004 and Pfiffner, 2016). Structural differences between the Central and Western Alps highlight the buttressing effect of the upper plate Ivrea body (see exp. B1). Wedging of the lower plate by the indenting lower crust of the upper plate in the Central Alps shows geometric similarities with experiment C1. Fold-like geometries at or close to the boundary between the lower and upper crust as shown in (j), suggest the prevalence of ductile deformation processes in deeper parts of the crust as predicted by our numerical experiments (e.g. Exp. A2, B2 and B1).

and tectonic position (lower vs. upper plate) of the colliding plates.

The Pyrenees is probably a viable example of an orogen where the lower plate might have been strong at the onset of collision. It follows the likely subduction of an intervening oceanic basin, where subcontinental mantle has been exhumed during Mid Cretaceous rifting (Lagabrielle et al., 2010; Jammes et al., 2010; Vissers and Meijer, 2012; Mouthereau et al., 2014). The Pyrenees mountain belt is characterized by an antiformal stack of Variscan basement units at its centre and a foreland propagating thin-skinned fold and thrust belt on either side of the axial zone (Roure et al., 1989; Muñoz, 1992; Fig. 8g). The antiformal stack of the axial zone is, furthermore, characterized by a gradual increase in steepness of the main foliation starting from north of the Orri dome to the North Pyreneean Fault, where foliations are subvertical (Zwart, 1986). This has resulted in the emplacement of lower plate (Iberian) Variscan basement thrusts sheets onto European crust (Fig. 8g). Our experiment C1 (Figs. 6, 8c) shows a similar crustal geometry due to the gradual rotation of thrust units during convergence. This rotation suggests that also in the case of the Pyrenees the subducting crust was coupled and strong, leading to the development of an antiformal stack. In addition, continued rotation of thrust units in C1 results in transfer of lower plate material onto the upper plate along a mid-crustal décollement, which is likely also the case in the Pyrenees (compare Fig. 8c and g). A comparison of the first order geometry of the Pyrenees and our experiment C1, thus, favours an interpretation, which invokes a strong subducting crust.

4.2.2. The role of first order decoupling horizons and lower crust deformation

The Alps and the Pyrenees dominantly consist of upper crust material (basement and sedimentary cover), which has been accreted in the course of subduction and subsequent collision (Roure et al., 1989; Schmid et al., 1996). The absence of lower crust exposure from the downgoing plate infers its subduction and implies a major decoupling horizon at the transition from lower to upper crust (see recent interpretation of the deep structure of the Western Alps by Schmid et al., 2017). Our experiments suggest that lower crust subduction is controlled by the rheology of the lithosphere and its degree of coupling (Figs. 2, 3, 6). If the lower crust is strong and coupled to the mantle, it will subduct (e.g., Fig. 3). When the lower crust is weak and decoupled from the mantle, it deforms in a ductile manner and accretes to form a wedge-shaped body at the contact with the upper plate (Figs. 2 and 4). In these situations, the lower crust of the upper plate thickens and is coupled to the evolving orogenic wedge (Fig. 2). Deformation and thickening of lower crust above the subducting mantle lithosphere by thrusting (e.g. Kissling et al., 2006) or ductile flow (Pfiffner, 2016) has been suggested for the western Alps and more recently for the Central Alps (Fry et al., 2010; Pfiffner, 2014). Although, the exact nature of lower crust deformation in these regions is still a matter of debate, geophysical data (Fry et al., 2010) and also our modelling results (Figs. 2 and Fig. 8) suggest that deformation and thickening of the subducting (European) lower crust is linked to the buttressing effect of the strong mantle wedge of the overriding plate.

The degree of crustal coupling and the distribution of decoupling horizons in the upper and lower plate is of key importance for the geometry, topography and length scale of the mountain belt. For example, strong coupling may lead to partial subduction of upper crust and the formation of high but narrow orogens with an antiformal stack structure at its centre (Fig. 7). When the crust of the lower plate is strong, the deformation front of the model mountain belt is stationary and can be directly linked to the suture zone at mantle depths (Figs. 6 and 7). In all other cases where the upper crust is strongly decoupled from the lower crust the model mountain belt is less high, but wider and deformation propagates far into the foreland. This behaviour is a fundamental mechanical condition for most collisional mountain belts and is consisted with lithospheric-scale analogue modelling experiments (Willingshofer et al., 2013).

Conversely, our experiments suggest that crustal decoupling in the weak upper plate creates retro-wedges (Figs. 6 and 7) as observed in the Alps and the Pyrenees and thus forms an important constraint for the rheological state of the overriding plate during collision.

5. Conclusions

We have analysed the impact of lateral strength contrasts on the dynamics of continent-continent collision zones. Our results indicate that differences in strength may result in a variety of different crustal geometries. Subduction of weak lithosphere beneath a strong upper plate leads to asymmetric deformation. The lower plate is subjected to intense shortening (upper crust) and continental subduction (lower crust), while the upper plate remains nominally undeformed. Thus, a clear correlation between plate strength and the localization of deformation (dominantly in the lower plate) exists. Such partitioning of deformation is observed, for example, in the Western Alps, where the Ivrea body acts as strong buttress against which lower plate material was accreted during the late stage of collision. In contrast, subduction of strong lithosphere beneath a weak upper plate results in a more complex deformation pattern. Deformation initiates on the lower plate and forms an antiformal stack, but moves into the undeformed upper plate during ongoing collision. Here, deformation is strongly linked to the kinematics of the colliding plates and no direct correlation between plate strength and the partitioning of upper plate-lower plate deformation exists. Similarly, in the Central Alps, the continued deformation of the lower plate was accompanied by deformation of the upper plate at later stages of collision. Another viable example of this process are the Pyrenees, where the presence of an antiformal stack in the axial zone of the orogen might be related to lower plate indentation at the onset of collision.

Acknowledgements

This work was supported by the Netherlands Research Centre of Integrated Solid Earth Sciences. All experiments were run on the Brutus cluster at ETH Zurich. We thank Adrian Pfiffner and Alexander Koptev for their insightful comments and Philippe Agard for handing the manuscript.

References

Beaumont, C., Quinlan, G., 1994. A geodynamic framework for interpreting crustal-scale seismic-reflectivity patterns in compressional orogens. Geophys. J. Int. 116 (3), 754–783.
Becker, T.W., Faccenna, C., 2011. Mantle conveyor beneath the Tethyan collisional belt. Earth Planet. Sci. Lett. 310, 453–461.
Bonini, M., Sokoutis, D., Talbot, C.J., Boccaletti, M., Milnes, A.G., 1999. Indenter growth in analogue models of alpine-type deformation. Tectonics 18 (1), 119–128.
Brun, J.-P., 2002. Deformation of the continental lithosphere: insights from brittle-ductile models. Geol. Soc. Lond., Spec. Publ. 200 (1), 355–370.
Burg, J.P., Gerya, T.V., 2005. The role of viscous heating in Barrovian metamorphism of collisional orogens: thermomechanical models and application to the Lepontine dome

in the central alps. J. Metamorph. Geol. 23 (2), 75–95.
Burov, E., Yamato, P., 2008. Continental plate collision, P–T–t–z conditions and unstable vs. stable plate dynamics: Insights from thermo-mechanical modelling. Lithos 103 (1–2), 178–204.
Burov, E., Francois, T., Yamato, P., Wolf, S., 2014. Mechanisms of continental subduction and exhumation of HP and UHP rocks. Gondwana Res. 25 (2), 464–493.
Calignano, E., Sokoutis, D., Willingshofer, E., Gueydan, F., Cloetingh, S., 2015. Asymmetric vs. symmetric deep lithospheric architecture of intra-plate continental orogens. Earth Planet. Sci. Lett. 424, 38–50.
Choukroune, P., 1989. The ECORS Pyrenean deep seismic profile reflection data and the overall structure of an orogenic belt. Tectonics 8 (1), 23–39.
Crespo-Blanc, A., González-Sánchez, A., 2005. Influence of indenter geometry on arcuate fold-and-thrust wedge: preliminary results of analogue modelling. Geogaceta 37, 11–14.
Davy, P., Cobbold, P., 1988. Indentation tectonics in nature and experiment: 1. Experiments scaled for gravity. Bull. Geologic. Inst. Univ. Uppsala 14, 129–142.
Diehl, T., Husen, S., Kissling, E., Deichmann, N., 2009. High-resolution 3-D P-wave mode of the Alpine crust. Geophys. J. Int. 179, 1133–1147.
Ellis, S., Schreurs, G., Panien, M., 2004. Comparisons between analogue and numerical models of thrust wedge development. J. Struct. Geol. 26 (9), 1659–1675.
England, P., Houseman, G., 1986. Finite strain calculations of continental deformation 2Comparison with the India-Asia collision zone. J. Geophys. Res. 91 (B3), 3664–3676.
England, P., McKenzie, D., 1982. A thin viscous sheet model for continental deformation. Geophys. J. R. Astron. Soc. 70 (2), 295–321.
Faccenda, M., Gerya, T.V., Chakraborty, S., 2008. Styles of post-subduction collisional orogeny: influence of convergence velocity, crustal rheology and radiogenic heat production. Lithos 103 (1–2), 257–287.
Fry, B., Deschamps, F., Kissling, E., Stehly, L., Giardini, D., 2010. Layered azimuthal anisotropy of Rayleigh wave phase velocities in the European Alpine lithosphere inferred from ambient noise. Earth Planet. Sci. Lett. 297 (1), 95–102.
Gerbault, M., Willingshofer, E., 2004. Lower crust indentation or horizontal ductile flow during continental collision? Tectonophysics 387 (1), 169–187.
Gerya, T., 2010. Introduction to Numerical Geodynamic Modelling. Cambridge University Press.
Gerya, T., Yuen, D., 2003. Characteristics-based marker-in-cell method with conservative nite-differences schemes for modeling geological flows with strongly variable transport properties. Phys. Earth Planet. Inter. 140 (4), 293–318.
Gerya, T., Yuen, D., 2007. Robust characteristics method for modelling multiphase visco elasto plastic thermo-mechanical problems. Phys. Earth Planet. Inter. 163, 83–105.
Gorczyk, W., Vogt, K., 2015. Tectonics and melting in intra-continental settings. Gondwana Res. 27 (1), 196–208.
Handy, M.R., Franz, L., Heller, F., Janott, B., Zurbriggen, R., 1999. Multistage accretion and exhumation of the continental crust (Ivrea crustal section, Italy and Switzerland). Tectonics 18 (6), 1154–1177.
Houseman, G., England, P., 1986. Finite strain calculations of continental deformation 1. Method and general results for convergent zones. J. Geophys. Res. 91 (B3), 3651–3663.
Jammes, S., Huismans, R.S., 2012. Structural styles of mountain building: controls of lithospheric rheologic stratification and extensional inheritance. J. Geophys. Res. Solid Earth 117 (B10).
Jammes, S., Tiberi, C., Manatschal, G., 2010. 3D architecture of a complex transcurrent rift system: the example of the Bay of Biscay–Western Pyrenees. Tectonophysics 489 (1), 210–226.
Jammes, S., Huismans, R.S., Muñoz, J.A., 2014. Lateral variation in structural style of mountain building: controls of rheological and rift inheritance. Terra Nova 26 (3), 201–207.
Keep, M., 2000. Models of lithospheric-scale deformation during plate collision: effects of indentor shape and lithospheric thickness. Tectonophysics 326, 203–216.
Kissling, E., Schmid, S.M., Lippitsch, R., Ansorge, J., Fügenschuh, B., 2006. Lithosphere structure and tectonic evolution of the Alpine arc: new evidence from high-resolution teleseismic tomography. Geol. Soc. Lond. Mem. 32 (1), 129–145.
Lagabrielle, Y., Labaume, P., de Saint Blanquat, M., Lagabrielle, Y., Labaume, P., de Saint Blanquat, M., 2010. Mantle exhumation, crustal denudation, and gravity tectonics during Cretaceous rifting in the Pyrenean realm (SW Europe): Insights from the geological setting of the lherzolite bodies. Tectonics 29 (4).
Lippitsch, R., Kissling, E., Ansorge, J., 2003. Upper mantle structure beneath the Alpine orogen from high-resolution teleseismic tomography. J. Geophys. Res. Solid Earth 108 (B8).
Liu, H., McClay, K.R., Powell, D., 1992. Physical models of thrust wedges. In: Thrust Tectonics. Springer, Netherlands, pp. 71–81.
Luth, S., Willingshofer, E., Sokoutis, D., Cloetingh, S., 2010. Analogue modelling of continental collision: influence of plate coupling on mantle lithosphere subduction, crustal deformation and surface topography. Tectonophysics 484 (1), 87–102.
Luth, S., Willingshofer, E., Sokoutis, D., Cloetingh, S., 2013a. Does subduction polarity changes below the Alps? Inferences from analogue modelling. Tectonophysics 582, 140–161.
Luth, S., Willingshofer, E., Borgh, M., Sokoutis, D., Otterloo, J., Versteeg, A., 2013b. Kinematic analysis and analogue modelling of the Passeier- and Jaufen faults: implications for crustal indentation in the Eastern Alps. Int. J. Earth Sci. 102 (4), 1071–1090.
Mouthereau, F., Filleaudeau, P.-Y., Vacherat, A., Pik, R., Lacombe, O., Fellin, M.G., Castelltort, S., Christophoul, F., Masini, E., 2014. Placing limits to shortening evolution in the Pyrenees: role of margin architecture and implications for the Iberia/Europe convergence. Tectonics 33, 2283–2314. http://dx.doi.org/10.1002/2014TC003663.
Muñoz, J.A., 1992. Evolution of a Continental Collision Belt: ECORS-Pyrenees Crustal Balanced Cross-Section. In: Thrust Tectonics. Springer, Netherlands, pp. 235–246.
Pfiffner, O.A., 2014. Geology of the Alps. John Wiley & Sons.
Pfiffner, O., 2016. Basement-involved thin-skinned and thick-skinned tectonics in the Alps. Geol. Mag. 153 (5–6), 1085–1109.
Pfiffner, O., Ellis, S., Beaumont, C., 2000. Collision tectonics in the Swiss Alps: insight from geodynamic modeling. Tectonics 19 (6), 1065–1094.
Ranalli, G., 1995. Rheology of the Earth. Springer.
Ratschbacher, L., Merle, O., Davy, P., Cobbold, P., 1991a. Lateral extrusion in the Eastern Alps, part 1: boundary conditions and experiments scaled for gravity. Tectonics 10 (2), 245–256.
Rosenberg, C.L., Kissling, E., 2013. Three-dimensional insight into Central-Alpine collision: lower-plate or upper-plate indentation? Geology 41 (12), 1219–1222.
Roure, F., Choukroune, P., Berastegui, X., Munoz, J.A., Villien, A., Matheron, P., Bareyt, M., Seguret, M., Camara, P., Deramond, J., 1989. ECORS deep seismic data and balanced cross sections: geometric constraints on the evolution of the Pyrenees. Tectonics 8 (1), 41–50.
Ruh, J.B., Kaus, B.J., Burg, J.P., 2012. Numerical investigation of deformation mechanics in fold-and-thrust belts: influence of rheology of single and multiple décollements. Tectonics 31 (3).
Schmid, S.M., Kissling, E., 2000. The arc of the western Alps in the light of geophysical data on deep crustal structure. Tectonics 19 (1), 62–85.
Schmid, S.M., Pfiffner, O., Froitzheim, N., Schönborn, G., Kissling, E., 1996. Geophysical geological transect and tectonic evolution of the Swiss-Italian Alps. Tectonics 15 (5), 1036–1064.
Schmid, S.M., Fügenschuh, B., Kissling, E., Schuster, R., 2004. Tectonic map and overall architecture of the Alpine orogen. Eclogae Geol. Helv. 97 (1), 93–117.
Schmid, S.M., Kissling, E., Diehl, T., van Hinsbergen, D.J., Molli, G., 2017. Ivrea mantle wedge, arc of the western alps, and kinematic evolution of the Alps–Apennines orogenic system. Swiss J. Geosci. 1–32.
Schneider, F.M., Yuan, X., Schurr, B., Mechie, J., Sippl, C., Haberland, C., Minaev, V., Oimahmadov, I., Gadoev, M., Radjabov, N., Abdybachaev, U., Orunbaev, S., Negmatullaev, S., 2013. Seismic imaging of subducting continental lower crust beneath the Pamir. Earth Planet. Sci. Lett. 375, 101–112.
Schoenbohm, L.M., Burchfiel, B.C., Liangzhong, C., 2006. Propagation of surface uplift, lower crustal flow, and Cenozoic tectonics of the southeast margin of the Tibetan plateau. Geology 34, 813–816.
Sokoutis, D., Willingshofer, E., 2011. Decoupling during continental collision and intraplate deformation. Earth Planet. Sci. Lett. 305 (3), 435–444.
Sokoutis, D., Burg, J.P., Bonini, M., Corti, G., Cloetingh, S., 2005. Lithospheric-scale structures from the perspective of analogue continental collision. Tectonophysics 406 (1), 1–15.
Teixell, A., 1998. Crustal structure and orogenic material budget in the west central Pyrenees. Tectonics 17, 395–406.
Toussaint, G., Burov, E., Jolivet, L., 2004. Continental plate collision: unstable vs. stable slab dynamics. Geology 32 (1), 33–36.
TRANSALP Working Group, 2002. First deep seismic reflection images of the Eastern Alps reveal giant crustal wedges and transcrustal ramps. Geophys. Res. Lett. 29 (10), 92.1–92.4.
Vissers, R.L.M., Meijer, P.T., 2012. Iberian plate kinematics and Alpine collision in the Pyrenees. Earth Sci. Rev. 114 (1), 61–83.
Vogt, K., Gerya, T.V., 2014. From oceanic plateaus to allochthonous terranes: numerical modelling. Gondwana Res. 25 (2), 494–508.
Vogt, K., Gerya, T., Castro, A., 2012. Crustal growth at active continental margins: numerical modeling. Phys. Earth Planet. Inter. 192-193, 1–20.
Vogt, K., Matenco, L., Cloetingh, S., 2017. Crustal mechanics control the geometry of mountain belts. Insights from numerical modelling. Earth Planet. Sci. Lett. 460, 12–21.
Wagner, M., Kissling, E., Husen, S., 2012. Combining controlled-source seismology and local earthquake tomography to derive a 3-D crustal model of the westernAlpine region. Geophys. J. Int. 191, 789–802.
Wang, Y., Chevrot, S., Monteiller, V., Komatitsch, D., Mouthereau, F., Manatschal, G., Sylvander, M., Diaz, J., Ruiz, M., Grimaud, F., Benahmed, S., 2016. The deep roots of the western Pyrenees revealed by full waveform inversion of teleseismic P waves. Geology 44 (6), 475–478.
Willingshofer, E., Cloetingh, S., 2003. Present-day lithospheric strength of the Eastern Alps and its relationship to neotectonics. Tectonics 22 (6).
Willingshofer, E., Sokoutis, D., 2009. Decoupling along plate boundaries: key variable controlling the mode of deformation and the geometry of collisional mountain belts. Geology 37 (1), 39–42.
Willingshofer, E., Sokoutis, D., Burg, J.-P., 2005. Lithospheric-scale analogue modeling of collision zones with a pre-existing weak zone. In: Gapais, D., Brun, J.P., Cobbold, P.R. (Eds.), Deformation Mechanisms, Rheology and Tectonics: from Minerals to the Lithosphere. Volume 243. Geol. Soc. London, Spec. Publ., pp. 277–294.
Willingshofer, E., Sokoutis, D., Luth, S., Beekman, F., Cloetingh, S., 2013. Subduction and deformation of the continental lithosphere in response to plate and crust-mantle coupling. Geology 41 (12), 1239–1242.
Zhao, L., Paul, A., Guillot, S., Solarino, S., Malusà, M.G., Zheng, T., Zhu, R., 2015. First seismic evidence for continental subduction beneath the Western Alps. Geology 43 (9), 815–818.
Ziegler, P.A., Cloetingh, S., van Wees, J.-D., 1995. Dynamics of intra-plate compressional deformation: the Alpine foreland and other examples. Tectonophysics 252, 7–22.
Ziegler, P.A., van Wees, J.-D., Cloetingh, S., 1998. Mechanical controls on collision-related compressional intraplate deformation. Tectonophysics 300, 103–129.
Zwart, H.J., 1986. The Variscan geology of the Pyrenees. Tectonophysics 129 (1–4), 919–1727.